

DEVELOPMENT OF A COUPLED FINITE ELEMENT AND MESH-FREE METHOD IN LS-DYNA

Cheng-Tang Wu¹, Mark E. Botkin² and Hui-Ping Wang²

¹ Livermore Software Technology Corporation
7374 Las Positas Road
Livermore, CA 94550
ctwu@lstc.com

² GM R & D Center
Mail Code 480-106-256
Vehicle Analysis and Dynamics Lab
Warren, MI 48090-9055
mark.e.botkin@gm.com, hui-ping.wang@gm.com

Keywords: mesh-free; finite element; integration constraint

Abbreviations:

RKPM : reproducing kernel particle method
EFG : element-free Galerkin
SCNI : stabilized conforming nodal integration

ABSTRACT

A coupled finite element and mesh-free method for the solid and structure analysis has been proposed. This method is developed to minimize the mesh distortion problems encountered in the finite element analysis and to reduce the high CPU cost associated with the mesh-free computation.

To couple the mesh-free method with the LS-DYNA, an *interface constraint* has been developed. This *interface constraint* is introduced onto the interfaces between finite element and mesh-free zones, and mesh-free and mesh-free zones. The completeness condition is imposed in the solution approximation to achieve the desired consistency across the interfaces.

To satisfy the linear exactness in the mesh-free Galerkin approximation of the Dirichlet boundary value problem, two *integration constraints* have been developed. A local boundary integration scheme has been proposed to satisfy the *first integration constraint* and to eliminate the possible hourglass modes. The *interface constraint* is further extended to the essential boundaries to meet *the second integration constraint* and to reduce the computation time on the imposition of essential boundary conditions. Several examples are solved to evaluate the numerical performance.

INTRODUCTION

Structures subjected to severe material distortion commonly exist in survivability, safety and manufacturing related applications in the defense, aerospace, and automotive industries. Typical examples in the automotive industry are vehicle crashes in frontal and side impact, fuel tanks subjected to impact load, and metal parts manufactured by forging or stamping processes. Despite its success in the analysis of geometric and material nonlinear behavior in structures and solids, the widely used finite element method exhibits a number of shortcomings in handling design problems involving large deformation, high gradients, localization, or moving discontinuities. These difficulties are partially due to the regularity requirement of mesh discretization. In the industrial community, this becomes one of the most challenging tasks in numerical simulations.

In recent years, classes of mesh-free methods have been developed for specific applications [1, 2, 13]. In these methods, the domain of interest is discretized by a scattered set of points. The uniqueness of the mesh-free methods is due to the development of new interpolation/shape functions that allow the interpolation of field variables to be accomplished at a global level without the usage of meshes. These methods are ideal for hp-adaptivity, fracture problems, multiple-resolution analysis, and large deformation problems. However, most of the mesh-free methods consume considerably higher CPU time than the finite element methods.

To resolve this problem, several mixed finite element and mesh-free methods have been proposed [3, 12, 15]. The objective is to use the advantages of each method. Belytschko et al. [3] first introduced a transit element that is of the size of one finite element and the linear interpolation of mesh-free. Wagner and Liu [16] proposed a corrected collection method. Those methods require an extra degree of freedoms for the coupling of the conventional finite element method and mesh-free method. Huerta et al. [12] revised Belytschko's approach and propose a mixed hierarchical approximation based on the element-free Galerkin method [2].

In this paper, we present a coupled finite element and mesh-free method in conjunction with the LS-DYNA [11] code for explicit dynamic analysis. This paper is organized as follows: In first part, the development of the coupled finite element and mesh-free method is described, and the required interface constraints and consistency conditions across interfaces are discussed. The second part presents the coupled finite element and mesh-free formulation for explicit dynamic analysis. Two integration constraints are developed to satisfy the linear exactness in the mesh-free Galerkin approximation of the Dirichlet boundary value problem. Numerical results are presented in the third part to demonstrate the effectiveness of this development, followed by conclusions and discussions.

A COUPLED FINITE ELEMENT AND MESH-FREE METHOD

To reduce the mesh distortion problems in standard finite element analysis, the mesh-free computation is added into the existing finite element based analysis model. The coupling of this mesh-free computation should be computationally efficient, with few modification of the original analysis model, and numerically consistent.

In conventional coupling methods, a layer of finite elements is added onto the interface between each finite element and mesh-free zone. The shape functions of those interface elements are comprised of the standard finite element and conventional mesh-free shape functions with the completeness condition imposed to satisfy the consistency. Nevertheless, these methods still require the structured interface elements and their performance are affected by the elements regularity.

To avoid the structured interface element requirement, an *interface constraint* is proposed. The idea of this proposed *interface constraint* is to introduce a strip of finite element 'nodes' (instead of using a layer of structured interface elements) on the interface between finite element and mesh-free zones, and mesh-free and mesh-free zones as shown in Figure 1. These additional nodes are taken to be the same nodes from the finite element based analysis model and do not require an extra degree of freedoms. As a result, the computation preserves the mesh-free unstructured characteristics, modification effort for the standard finite element based analysis model is minimized, and the computation can be efficient.

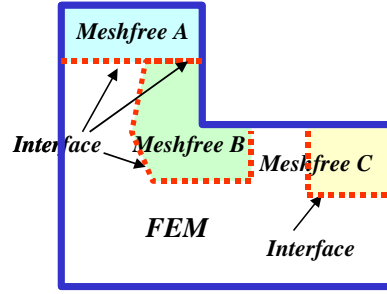


Figure 1. A two-dimensional FEM analysis model with three added mesh-free computation zones: Mesh-free A, B and C and four corresponding interfaces.

Derivation of the coupled finite element and mesh-free method is presented in following section. At first, the mesh-free approximations are constructed based on the framework of moving least-squares interpolation. The element-free Galerkin method (EFG) [2] and the reproducing kernel particle method (RKPM) [13] are two representatives of moving least-squares approximation. In this study, we formulate the mesh-free approximation by the RKPM. According to the proposed idea, the discrete solution approximation at a point \mathbf{x} is obtained as

$$u_i(\mathbf{x}) \approx u_i^h(\mathbf{x}) = \begin{cases} \sum_{x_L \in \Omega_{FEM}}^{KP} \Phi_L^{[m]}(\mathbf{x}; \mathbf{x} - \mathbf{x}_L) d_{iL}; \forall \mathbf{x} \in \Omega_{FEM} \subset \mathbf{R}^d \\ \sum_{x_I \in \Omega_{Meshfree}}^{NP} \bar{w}_a^{[n]}(\mathbf{x}; \mathbf{x} - \mathbf{x}_I) d_{iI} + \sum_{x_L \in \Gamma_{Interface}}^{MP} \Phi_L^{[m]}(\mathbf{x}; \mathbf{x} - \mathbf{x}_L) d_{iL}; \forall \mathbf{x} \in \Omega_{Meshfree} \subset \mathbf{R}^d \end{cases} \quad (1)$$

where Ω_{FEM} denotes the sub-domain for the finite element computation and $\Omega_{Meshfree}$ is the sub-domain for mesh-free computation. $\Omega := \Omega_{FEM} \cup \Omega_{Meshfree}$ is a bounded domain in \mathbf{R}^d and $\Gamma_{Interface} := \Omega_{FEM} \cap \Omega_{Meshfree}$ is the interface between the finite element and mesh-free sub-domains or the interface between any two mesh-free sub-domains.

$\bar{w}_a^{[n]}$ is called the reproducing kernel function, and is usually expressed by a linear combination of n -th order local basis functions and a compact support kernel function; $[n]$ denotes the order of basis functions and 'a' is the support size of the kernel. $\Phi_L^{[m]}$ is the standard finite element shape function with order of interpolation $[m]$. NP is the total number of mesh-free particles that influence the solution at point \mathbf{x} . KP is the total number of the finite element nodes per element when point \mathbf{x} is located inside the finite element zones. d_{iI} is the coefficient of the approximation, and in general is not equivalent to the physical displacement. MP is the total number of the finite element nodes on the interface that influence the approximation.

Using the following reproducing conditions [14], one can restore the polynomials to a specific order by requiring the zero-th moment [14] to be one, and the higher order moments to be zero. The reproducing condition also refers to the completeness condition of an approximation, and is important for the convergence in the Galerkin methods.

$$\sum_{x_I \in \Omega_{Meshfree}}^{NP} \bar{w}_a^{[n]}(\mathbf{x}; \mathbf{x} - \mathbf{x}_I) x_{1I}^i x_{2I}^j + \sum_{x_J \in \Gamma_{Interface}}^{MP} \Phi_J^{[m]}(\mathbf{x}; \mathbf{x} - \mathbf{x}_J) x_{1J}^i x_{2J}^j = x_1^i x_2^j, \quad i + j = 0, \dots, n \quad (2)$$

Comment:

It is important to notice that, in most cases, the order of finite element interpolation $[m]$ is chosen to be the same as the reproducing order $[n]$, and the approximation is continuous everywhere in $\Omega_{Meshfree}$. If the reproducing order $[n]$ is larger than the finite element interpolation order $[m]$, i.e. $n > m$, then continuity is preserved only in $\Omega_{Meshfree} \setminus \Gamma_{Interface}$. Thus, discontinuities in the approximation are induced along $\Gamma_{Interface}$.

Satisfaction of the reproducing conditions in Equation (2) leads to the following coupled finite element and mesh-free solution approximation with the n -th order solution completeness.

$$u_i^h(\mathbf{x}) = \sum_{x_I \in \Omega_{Meshfree}}^{NP} \tilde{\Psi}_I(\mathbf{x})d_{II} + \sum_{x_J \in \Gamma_{Interface}}^{MP} \Phi_J^{[m]}(\mathbf{x})d_{IJ} = \sum_{x_I \in \Omega_{Meshfree}}^{NP} \hat{\Psi}_I(\mathbf{x})d_{II} \quad (3)$$

where

$$\begin{aligned} \tilde{\Psi}_I(\mathbf{x}) = & \sum_{x_I \in \Omega_{Meshfree}}^{NP} \{ \mathbf{H}^{[n]T}(\mathbf{0})\mathbf{M}^{[n]^{-1}}(\mathbf{x})\mathbf{H}^{[n]}(\mathbf{x} - \mathbf{x}_I) \\ & - \sum_{x_J \in \Gamma_{Interface}}^{MP} \mathbf{H}^{[n]T}(\mathbf{x} - \mathbf{x}_J)\mathbf{M}^{[n]^{-1}}(\mathbf{x})\mathbf{H}^{[n]}(\mathbf{x} - \mathbf{x}_I)\Phi_J^{[m]}(\mathbf{x}; \mathbf{x} - \mathbf{x}_J) \} w_a(\mathbf{x} - \mathbf{x}_I)d_{II} \end{aligned} \quad (4)$$

$\tilde{\Psi}_I$ is the reproducing kernel function corresponding to the mesh-free node I , and $\Phi_J^{[m]}$ is the standard finite element shape function associated with the finite element node J . $\hat{\Psi}_I$ is the modified coupled finite element and mesh-free shape function for the node I .

It has been shown by Wu [18] that for Equation (1) to be conforming across any interface, a necessary condition is required which is

$$\tilde{\Psi}_I(\mathbf{x}) = 0 \text{ for all nodes } \{I : \text{supp}(\Psi_I) \cap \Gamma_{Interface} \neq \emptyset\} \text{ and } \mathbf{x} \in \Gamma_{Interface} \quad (5)$$

We call Equation (5) the **interface constraint**. In other words, the shape functions on the interface between the finite element and mesh-free zones are reduced to standard finite element shape functions and pose the Kronecker delta property. Therefore, there is no non-conforming problem for the shape functions across the interface.

When $\mathbf{x} \in \Omega_{Meshfree} \setminus \Gamma_{Interface}$, and $n = m$ in Equation (2), the solution approximation will still meet the m th-order reproducing conditions.

FORMULATION FOR EXPLICIT DYNAMIC ANALYSIS

In this section, solution of the governing equations using the proposed coupled finite element and mesh-free approximation is achieved under the framework of the Galerkin weighted residual method. To satisfy the linear exactness in the Galerkin approximation, two integration constraints are introduced. A new mesh-free approximation is developed based on these two integration constraints, and a spatial integration scheme is introduced for the domain integration.

Recall the Lagrangian partial differential equation of motion

$$\rho \ddot{\mathbf{u}} = \nabla \cdot \boldsymbol{\sigma} - \mathbf{f}_b \text{ in } \Omega, \quad \Omega = \Omega_{FEM} \cup \Omega_{Meshfree} \quad (6)$$

with the divergence operator ∇ , the body force \mathbf{f}_b , and the essential and natural boundary conditions

$$\begin{aligned} \mathbf{u} &= \mathbf{u}_0 \text{ on } \Gamma_g \\ \boldsymbol{\sigma} \cdot \mathbf{n} &= \mathbf{h} \text{ on } \Gamma_h \end{aligned} \quad (7)$$

and with initial conditions

$$\begin{aligned} u(X,0) &= u^0(X) \\ \dot{u}(X,0) &= \dot{u}^0(X) \end{aligned} \quad (8)$$

The left side of Equation (6) is the material time derivative and will involve convective terms if the Eulerian kernel functions are used. To avoid the tensile instability caused by the Eulerian kernel functions [4], the Lagrangian kernel functions are implemented in this study.

To solve this set of partial differential equations with the Galerkin method (which is considered as standard for the development in the finite elements based on the displacement method), the equilibrium in its strong form of Equations (6)-(8) is weighted with some test functions defined by $W = \{w/w \in L^2(\Omega), w=0 \text{ on } \Gamma_g\}$. The corresponding weak form of Equation (6)-(8) becomes:

$$\int_{\Omega_x} \rho w \ddot{u} d\Omega = \int_{\Omega_x} w \cdot \nabla \cdot \sigma d\Omega - \int_{\Omega_x} w \cdot f_b d\Omega - \int_{\Gamma_h} w \cdot h d\Gamma \quad (9)$$

with

$$\begin{aligned} u(X,0) &= u^0(X) \\ \dot{u}(X,0) &= \dot{u}^0(X) \end{aligned} \quad (10)$$

The next step in the discretization is to choose a finite dimensional subspace $U^h \subset U$ with basis $\hat{\Psi}_I (I = 1 \dots n)$. $\hat{\Psi}_I (I = 1 \dots n)$ are the shape functions obtained from Equation (1). To this end, the basis of weighted functions is chosen to be the same as the trial functions after the spatial discretization. Since we choose the weighted functions to be in $H_0^1(\Omega)$, we can integrate by parts and obtain the discrete Galerkin weighted residual formulation. The references for the detailed derivation of weak equations and the imposition of essential boundary conditions using kinematically admissible mesh-free shape functions can be found in [5-7, 17]. Following the derivation for explicit time integration, the equations to be solved have the form

$$\hat{\alpha}^T A^{-T} M A^{-1} \hat{u} = \hat{\alpha}^T A^{-T} R^{int} \quad (11)$$

where

$$\begin{aligned} \hat{u}_I &= [\ddot{d}_{1I}, \ddot{d}_{2I}]^T \\ M_{IJ} &= \int_{\Omega_x} \rho \hat{\Psi}_I(x) \hat{\Psi}_J(x) d\Omega = \int_{\Omega_x} \rho^0 \hat{\Psi}_I(X) \hat{\Psi}_J(X) d\Omega \\ R_I &= \int_{\Omega_x} B_I^T(x) \cdot \sigma d\Omega - [\hat{\Psi}_I(x) h] \Big|_{\Gamma_h} - \int_{\Omega_x} \hat{\Psi}_I(x) f_b d\Omega \end{aligned} \quad (12)$$

and

$$\hat{u} = Au; A_{IJ} = \hat{\Psi}_J(X_I) \quad (13)$$

Usually, the numerical integration in Equation (11) is evaluated by Gauss quadrature using the so-called background mesh. However, the Gauss integration method fails to satisfy the linear exactness in the mesh-free Galerkin approximation of a second-order partial differential equation. Moreover, a higher order quadrature rule is often required for better accuracy, and this is one of the major causes of high CPU consumption in mesh-free methods. For convergence reasons, an *integration constraint* is required as a necessary condition for the linear exactness in the mesh-free Galerkin approximation of Dirichlet boundary value problems [9, 10]. Here, we call this the *first integration constraint* and it is given by

$$\int_{\Omega} B_I^T d\Omega = 0 \text{ for all interior nodes } \{I : \text{supp}(\hat{\Psi}_I) \cap \Gamma_{\text{boundary}} = 0\} \quad (14)$$

or in the discrete form,

$$\sum_{J=1} \nabla \hat{\Psi}_I(\mathbf{x}_J) A_J = \mathbf{0} \quad \text{for all interior nodes } \{I : \text{supp}(\tilde{\Psi}_I) \cap \Gamma_{\text{boundary}} = \emptyset\} \quad (15)$$

where \mathbf{B}_I is the gradient matrix; A_J is the weight of the domain integration point.

To meet this integration constraint, a stabilized conforming nodal integration method (SCNI) [9, 10] has been proposed. This method was originally designed as a strain smoothing stabilization in the strain localization analysis [8]. The method was further extended to minimize the integration errors and improve the computation inefficiency in the conventional mesh-free higher-order Gauss integration method.

From our numerical studies we observed that SCNI fails to satisfy the linear exactness in the cases when the supports of inner nodes cover the essential boundary nodes. In other words, the solution fails to display a linear displacement field in the Galerkin approximation of Dirichlet boundary value problem if $\exists \{\mathbf{x}_I\}$ for $\{I : \text{supp}(\Psi_I) \cap \Gamma_g \neq \emptyset\}$.

Therefore the satisfaction of *first integration constraint* is said to have passed a 'weak' linear exactness test. Wu [18] has further proved that for the mesh-free solution to satisfy the linear exactness test, an additional integration constraint is required.

$$\sum_{M=1} \hat{\Psi}_M(\mathbf{x}_N) \mathbf{x}_N = \mathbf{0} \quad \forall \mathbf{x}_N \in \Gamma_g \text{ and } \mathbf{x}_M \in \Omega_{\text{Meshfree}} \setminus \Gamma_g \quad (16)$$

We call Equation (16) the *second integration constraint*. It can be proved that the conventional mesh-free shape function and the coupled shape function $\hat{\Psi}_I$ in Equation (3) do not meet this requirement and therefore fails to satisfy the linear exactness in the mesh-free Galerkin approximation of Dirichlet boundary value problem. Moreover, the calculation of Equation (11) and the generalized displacement in Equation (13) by the conventional mesh-free approximation requires additional efforts for the matrix multiplication during each time step. Therefore, much higher computation time is expected in the implicit calculation. This is another major cause of high CPU usage for the mesh-free method.

To resolve the problem in the violation of the *second integration constraint*, and to improve the inefficiency in the calculation of Equations (11) and (13), the *interface constraint* concept is extended to the imposition of essential boundary conditions and contact conditions. By further extending similar constraint from interface to boundary, the solution approximation in the mesh-free zone is modified as

$$u_i^h(\mathbf{x}) = \sum_{x_I \in \Omega_{\text{Meshfree}}}^{NP} \bar{w}_a^{l m I}(\mathbf{x}; \mathbf{x} - \mathbf{x}_I) d_{il} + \sum_{x_I \in \Gamma_{\text{boundary}}}^{MP} \Phi_L^{l m I}(\mathbf{x}; \mathbf{x} - \mathbf{x}_I) d_{il} = \sum_{x_I \in \Omega_{\text{Meshfree}}}^{NP} \bar{\Psi}_I(\mathbf{x}; \mathbf{x} - \mathbf{x}_I) d_{il} \quad (17)$$

$\forall \mathbf{x} \in \Omega_{\text{Meshfree}}; \Gamma_{\text{interface}} \subset \Gamma_{\text{boundary}}$

It has been proven [18] that this new solution approximation satisfies the *second integration constraint*.

Another major shortcoming of the SCNI method is its inability to couple the mesh-free method with the finite element method. This is because the SCNI method is a nodal integration method, and all the quantities are computed and assigned to the nodes. As a result, internal variables such as strains and stresses evaluated at the interface nodes between finite element and mesh-free zones, and mesh-free and mesh-free zones are inconsistent. Moreover, from our numerical studies, it is also shown that the SCNI method displays hourglass modes when the support size is small or a high order basis function is adopted in the analysis.

In order to avoid the undefined nodal quantities on the interface and also to eliminate possible hourglass modes observed in the SCNI method, a modified local boundary integration method is introduced in this research for the domain integration. This method is equivalent to the two points Gauss integration with local boundary integration performed on each gauss point. For a more detailed derivation on the modified local boundary integration method see Wu [18].

To introduce the strain smoothing formulation into the Galerkin approximation, the mixed variational principle based on an assumed strain method is considered [9, 10]. Substituting the displacement and smoothed strain approximations into Equation (11) and performing the local boundary integration method [18], the discrete system equation becomes

$$\mathbf{M}\ddot{\mathbf{u}} = \mathbf{f}^{ext} - \mathbf{f}^{int}(\hat{\nabla}\mathbf{u}_i^h) \quad (18)$$

In the explicit dynamic analysis, a lumped mass matrix is considered for the computation efficiency. In this study, a row-sum method is used for the construction of the lumped mass matrix. Recall the consistent mass matrix in Equation (12), and perform the row-sum method, the diagonalized mass vector is given as

$$\mathbf{M}_I^{lump} = \sum_{J=1} \mathbf{M}_{IJ} = \int_{\Omega_x} \rho^0 \bar{\Psi}_I(\mathbf{X}) \sum_{J=1} \bar{\Psi}_J(\mathbf{X}) d\Omega = \int_{\Omega_x} \rho^0 \bar{\Psi}_I(\mathbf{X}) \quad (19)$$

The discrete form of \mathbf{f}_I^{int} in Equation (18) is

$$\mathbf{f}_I^{int}(\hat{\nabla}\mathbf{u}_i^h) = \sum_{IE=1}^{NE} \sum_{g=1}^{n_{int}} \bar{\mathbf{B}}_I^T(\mathbf{X}_g) \bar{\mathbf{G}}^T \cdot \bar{\boldsymbol{\sigma}}(\bar{\mathbf{F}}(\mathbf{x}_g)) \bar{\mathbf{J}}(\mathbf{X}_g) A_g \quad (20)$$

where $\bar{\mathbf{G}}^T$ is the transform matrix of the inverse of the smoothed deformation gradient for the usage of Lagrangian kernel function. For example, in a two-dimensional problem

$$\bar{\mathbf{G}}^T = \begin{bmatrix} \bar{F}_{11}^{-1} & 0 & \bar{F}_{21}^{-1} & 0 \\ 0 & \bar{F}_{22}^{-1} & 0 & \bar{F}_{12}^{-1} \\ \bar{F}_{12}^{-1} & \bar{F}_{21}^{-1} & \bar{F}_{22}^{-1} & \bar{F}_{11}^{-1} \end{bmatrix} \quad (21)$$

NUMERICAL EXAMPLES

Helmholtz Equation

To evaluate the performance of the proposed method, the Helmholtz equation is solved. In general, the Helmholtz equation considers the wave equation for cases where all data are simple-harmonic. The Helmholtz equation admits the family of localized asymptotic solutions, which are globally free of singularities, and usually provides an effective tool to study the integration representation of high frequency wave fields.

In this research, we consider the following one-dimensional Helmholtz equation with dimensionless unit given by

$$\nabla^2 u(x) + k^2 u(x) = 0, \text{ on } \Omega = \{x/0 \leq x \leq 2.5\} \quad (22)$$

with Dirichlet boundary conditions.

$$u(0) = 1, u(2.5) = 0 \quad (23)$$

where ∇^2 is the Laplacian, k is the wave number. For imaginary k , the equation becomes the spatial part of the diffusion equation. For real k , the solution of Helmholtz equation represents the spatial part of the wave equation. When k is zero, the equation reduces to the Laplace equation.

In this example, twelve uniformly distributed particles with the wave number equal to one and three are studied respectively. The particle number is chosen such that the discretization is close to the Nyquist limit and waves are allowed to propagate. The effect of the mesh-free approximation order is also considered. For the basis function

order of one, normalized kernel function support of 1.5 is used; for the basis function order of two, normalized support of 2.5 is used. Comparisons between the consistent mass and lumped mass formulations are made.

When the wave number is one, the displacements obtained from the consistent mass and lumped mass formulations match the analytical solution very well for two different approximation orders as shown in Figure 2. The square symbol denotes the results with the consistent mass formulation, the triangular symbol represents the results with the lumped mass formulation, and the solid line is the analytical solution.

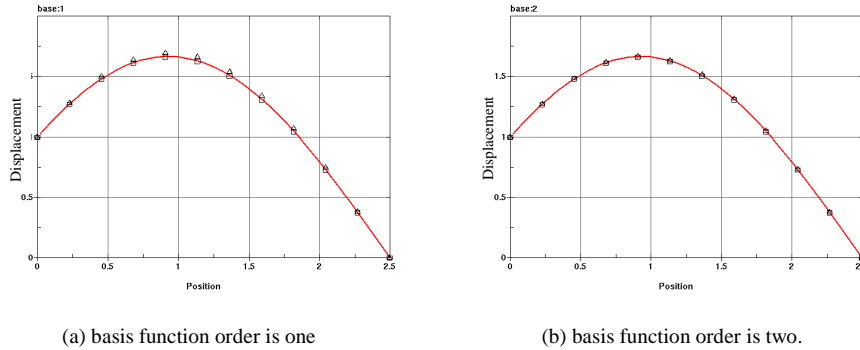


Figure 2. Displacement comparisons between consistent mass and lumped mass when the wave number is equal to one

Figure 3 shows, for higher wave number ($k = 3$) with approximation order equal to one, the consistent mass formulation still provides good performance whereas the solution obtained from the lumped mass loses some accuracy. By adding more particles, the discretization error in the lumped mass method could be minimized. Alternatively, the accuracy could also be improved by using higher order basis functions as shown in Figure 3 (b).

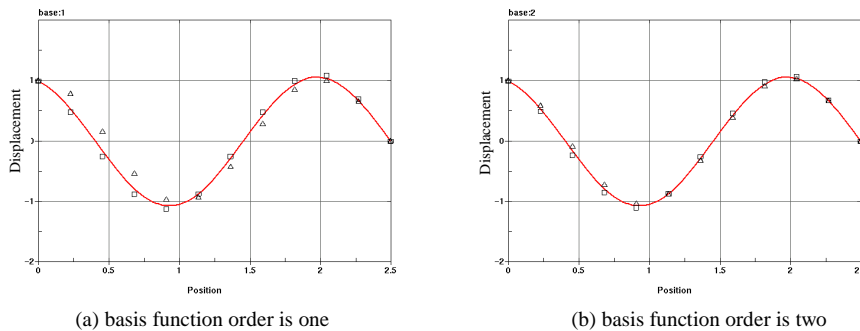


Figure 3. Displacement comparisons between consistent mass and lumped mass when the wave number is equal to three

Frictional Forging

This problem is studied to identify the applicability of the coupled finite element and mesh-free method to path-dependent materials with frictional contact conditions. A metal work piece compressed by a cylindrical punch as described in Figure 4 is analyzed. The plane-strain condition is considered. The punch is treated as a rigid body, and only the work piece is considered to be deformable. The material properties of the work piece are: initial density = $10E-3 \text{ lbf} \cdot \text{s}^2 / \text{in}^4$, Young's modulus = $6.825E7 \text{ psi}$, Poisson's ratio = 0.3 , and $J2$ perfect plasticity with yield stress

= 6000.0 psi. The friction coefficient between the work piece and punch is assumed to be 0.2. The velocity for the punch is 0.01 in/s. One mesh-free zone and the corresponding interface are added into the finite element based analysis model. Conventional finite element analysis is also conducted for comparison.

The analysis by the finite element method fails when severe mesh distortion occurs near the corner of the cylindrical punch as shown in Figure 4. The corresponding effective plastic strain is plotted in Figure 5. It is shown that finite element analysis displays a high level of effective plastic strains due to the tangled elements. As a result, a high level of stress concentration is expected in the conventional finite element analysis. On the other hand, the coupled finite element and mesh-free method effectively avoids the mesh tangling and provides smooth strain and stress distribution as shown in Figure 4 and 5. The progressive deformation obtained from the coupled finite element and mesh-free method is illustrated in Figure 6.

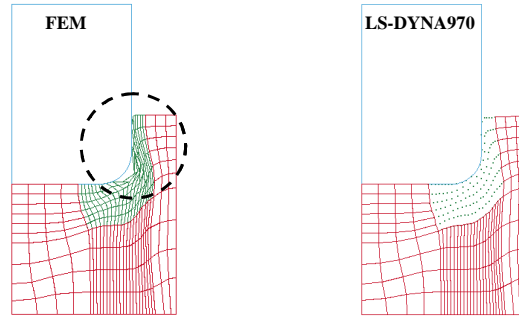


Figure 4. Comparison of deformed shapes.

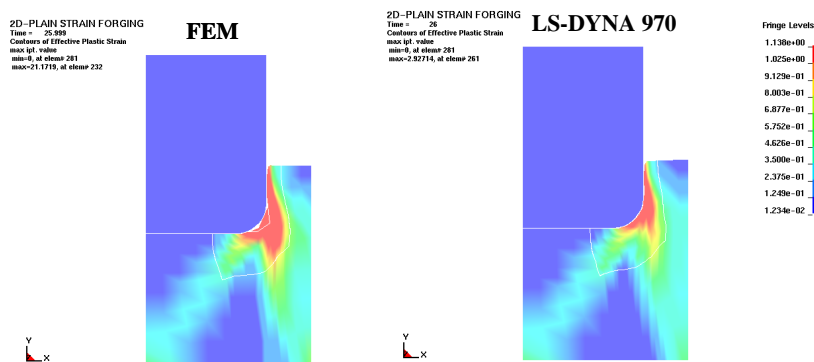


Figure 5. Comparison of effective plastic strain distribution.

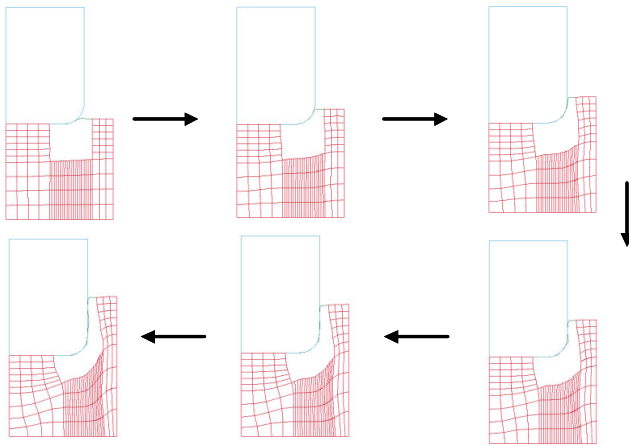


Figure 6. Progressive deformation by LS-DYNA 970.

CONCLUSION

To efficiently assess structural survivability, reusability and manufacturing for the industrial applications using simulation technology, a coupled finite element and mesh-free computational method is proposed for effective and realistic simulation of severe material deformation in structures.

To couple the mesh-free method with LS-DYNA, an *interface constraint* has been developed. To satisfy the linear exactness in the mesh-free Galerkin approximation of the Dirichlet boundary value problem, two *integration constraints* have been developed. A local boundary integration scheme with the coupled finite element and mesh-free shape function has been developed to satisfy the two *integration constraints*, to eliminate the possible hourglass modes and to reduce the computation time on the imposition of essential boundary conditions.

This method has been shown to perform well for explicit dynamics problems. The extension of this method to implicit analysis and shell formulation is under investigation.

ACKNOWLEDGEMENT

The support for this work by General Motors Corporation under contract TCS-12002 to LSTC is gratefully acknowledged.

REFERENCES

1. Babuska, I. and Melenk, J. M. (1996). "The Partition of Unity Method." *Int. J. Numer. Meth. Eng.*, Vol. 40, pp-727-758.
2. Belytschko, T., Lu, Y. Y. and Gu, L. (1994). "Element-Free Galerkin Methods." *Int. J. Numer. Meth. Eng.*, Vol. 37, pp-229-256.
3. Belytschko, T., Organ, D., and Kronggauz, Y. (1995). "A Coupled Finite Element- Element-Free Galerkin Method." *Computational Mechanics*, Vol. 51, pp-221-258.
4. Belytschko, T., Guo, Y., Liu, W. K., and Xiao, S. P. (2000). "A Unified Stability Analysis of Meshless Particle Methods." *Int. J. Numer. Meth. Eng.*, Vol. 48, pp-1359-1400.
5. Chen, J. S., Pan, C., Wu, C. T. and Liu, W. K. (1996). "Reproducing Kernel Particle Methods for Large Deformation Analysis of Nonlinear Structures." *Comput. Meth. Appl. Mech. Engng.*, Vol. 139, pp-195-227.
6. Chen, J. S. and Wang, H. P. (2000). "Some Recent Improvements in Meshfree Methods for Incompressible Finite Elasticity Boundary Value Problems with Contact." *Computational Mechanics*, Vol. 25, pp-137-156.
7. Chen, J. S. and Wang, H. P. (2000). "New Boundary Condition Treatments for Meshless Computation of Contact Problems." *Comput. Meth. Appl. Mech. Engng.*, Vol.187, pp-441-468.
8. Chen, J. S., Wu, C. T. and Belytschko, T. (2000). "Regularization of Material Instabilities by Meshfree Approximations with Intrinsic Length Scales." *Int. J. Numer. Meth. Eng.*, Vol. 47, pp-1303-1322.
9. Chen, J. S., Wu, C. T., Yoon, S., and You, Y. (2001). "A Stabilized Conforming Nodal Integration for Galerkin Meshfree Methods." *Int. J. Numer. Meth. Eng.*, Vol. 50, pp-439-466.
10. Chen, J. S., Yoon, S. and Wu, C. T. (2002). "Nonlinear Version of Stabilized Conforming Nodal Integration for Galerkin Meshfree Methods." *Int. J. Numer. Meth. Eng.*, Vol. 52, pp-2587-2615.
11. Hallquist, J. O. (2002). "LS-DYNA." Livermore Software Technology Corporation.
12. Huerta, A. and Fernandez-Mendez S. (2000). "Enrichment and Coupling of the Finite Element and Meshless Methods." *Int. J. Numer. Meth. Eng.*, Vol. 48, pp-1615-1636.
13. Liu, W. K., Jun, S., and Zhang, Y. F. (1995). "Reproducing Kernel Particle Methods." *Int. J. Numer. Meth. Fluids*, Vol. 20, pp-1081-1106.
14. Liu, W. K., Jun, S., Li, S., Adee, J., and Belytschko, B. (1995). "Reproducing Kernel Particle Methods for Structural Dynamics." *Int. J. Numer. Meth. Eng.*, Vol. 38, pp-1655-1679.
15. Liu, W. K., Uras R. A. and Chen, Y. (1997). "Enrichment of the Finite Element Method with Reproducing Kernel Particle Methods." *Journal of Applied Mechanics*, Vol. 64, pp-861-870.
16. Wagner, G. J. and Liu, W. K. (2000). "Application of Essential Boundary Conditions in Mesh-free Methods: A Corrected Collection Method," *Int. J. Numer. Meth. Eng.*, Vol. 47, pp-1367-1379.
17. Wu, C. T., Chen, J. S., Chi, L. and Huck, F. (2001). "A Lagrangian Meshfree Formulation for Analysis of Geotechnical Materials." *Journal of Engineering Mechanics*, Vol. 127, pp-440-449.
18. Wu, C. T. (2002). "Improvements of Mesh-free Galerkin Method for Structural Analysis." Internal Report, LSTC.

